Research Paper

Impact behavior of droplets on slippery liquid-infused porous surface under elevated temperatures

Chuchen Yue [ORCID], Qingwen Dai [*], Wei Huang , Xiaolei Wang [ORCID]

National Key Laboratory of Helicopter Aeromechanics, Nanjing University of Aeronautics and Astronautics, Nanjing 210016, China
College of Mechanical and Electrical Engineering, Nanjing University of Aeronautics and Astronautics, Nanjing 210016, China

ARTICLE INFO

ABSTRACT

Slippery liquid-infused porous surfaces have broad applications due to their excellent properties, but their performance under high-temperature conditions typical in industry remains underexplored. In this study, textured and slippery surfaces were fabricated via ultraviolet laser processing and chemical modification. The impact behaviors of water, mixture, and emulsion droplets on smooth, textured, and slippery surfaces were examined from 130 to 230 °C. Evaporation experiments revealed notably lower static Leidenfrost points for droplets on slippery surfaces—180, 180, and 190 °C for water, mixture, and emulsion, respectively—demonstrating the thermal stability of the slippery surface. Impact mode maps summarized droplet behaviors, and dynamic Leidenfrost points were identified, with water droplets showing values of 160, 160, 190, 130, and 130 °C across five surfaces at impact velocity $V = 0.9$ m/s. Changes in spreading factor and schematics elucidated that co-evaporation of lubricant and water stabilizes the vapor layer and enhances droplet bouncing. Numerical simulations revealed shorter solid–liquid contact times and clarified mechanisms of explosive bounce due to vapor flow variations among surface structures. Thermal resistance and heat transfer models for different surfaces were innovatively developed. These findings fill gaps in prior research lacking thermal considerations and offer theoretical insights for applications in surface self-cleaning, droplet manipulation, and thermal management.

1. Introduction

The droplet impact behavior on solid surfaces plays a critical role in a wide range of engineering applications, including self-cleaning [1], spray cooling [2], fuel injection [3], and liquid manipulation [4,5]. High-temperature operating conditions are extensively experienced in industries, and the droplet impact dynamics directly affect the system's heat and mass transfer efficiencies. For instance, the droplet deposition enhances the heat transfer efficiency, while the bounce can facilitate the mass transfer [6,7]. The Leidenfrost effect [8] is essential in mitigating energy loss, scaling, and corrosion [9,10], wherein the droplets are prevented from making direct contact with the high-temperature surfaces due to the rapid formation of a vapor layer.

The impact of droplets on high-temperature surfaces encompasses intricate thermodynamic and liquid dynamics principles, influenced by several factors, including surface wettability and morphology, droplet properties, and temperature difference. Tran et al. [11] investigated the boiling modes of water droplets on smooth hydrophilic silicon plates at temperatures ranging from 200 to 600 °C and classified them as contact boiling, gentle film boiling, and spraying film boiling. They observed that surface wettability governs the solid–liquid contact mode, thereby influencing the heat transfer characteristics. Guo et al. [12] employed infrared imaging to monitor the overall temperature variations of water droplets bouncing off high-temperature superhydrophobic surfaces. They formulated a transient heat flux model at the droplet-wall interface and established a positive correlation between cooling efficiency and *We* (the Weber number). In addition to the above planes, the impact of droplets on high-temperature pyramids [13], conical arrays [14], spheres [15], etc., shows a similar pattern.

Surface textures were observed to control the vapor flow beneath droplets. Zhang et al. [16] studied six impact modes of water droplets: wetting, contact boiling, transition, fracture, rebound, and partial rebound by manipulating surface wettability through micro-columns of varying specifications and graphene coatings. Liu et al. [17] compared the impact behavior of droplets on hydrophilic columnar and honeycomb arrays within a temperature range of 160–420 °C. A unique, rapid

pancake-like levitation was reported, which notably minimized the solid–liquid contact time. By altering the vapor flow patterns, Jiao et al. [18,19] engineered superhydrophobic textured surfaces and laser-ablated microgroove tool surfaces to suppress the Leidenfrost behavior of liquid droplets. They further demonstrated that microporous surfaces with negative slopes exhibited superior heat dissipation performance, highlighting the significant potential of negatively sloped surfaces in high-density thermal management applications [20].

Mixing of water with other liquids alters its physical properties, and water–oil mixtures and emulsions, in particular, are commonly found in many industrial applications. Blanken et al. [21] investigated the impact behavior of water-in-oil compound droplets on solid surfaces and observed that the water core of the compound droplet rebounded below a certain impact velocity, which is different from that of water droplets. This phenomenon is attributed to the oil shell, which serves as a lubricant and prevents direct contact between the water core and the solid surface. What's more, Cai et al. [22] explored the Leidenfrost dynamics of an impacting droplet of water and 2–8 vol% *iso*-propanol-water solutions in the film boiling regime up to 450 °C. They found that the isopropanol additive markedly enhanced the droplet spreading ability, which was speculated to be caused by lower surface energy. A similar behavior was observed with the emulsion droplet [23,24].

Recently, the impact behavior of droplets on various surfaces, particularly the slippery liquid-infused porous surfaces (SLIPS), has gained growing attention from researchers. Inspired by the micro-nanostructures and lubricating fluids in the inner wall of the pitcher plant, Wong et al. [25] first introduced the concept of SLIPS (i.e., coating a layer of ultra-thin lubricating oil on a substrate with micro-nanostructures) in 2011, which owns low liquid sliding resistance, low adhesion, and anti-pollution properties. SLIPS have been used in a wide range of applications, including condensation [26,27], liquid and fog harvesting [28,29], and surface self-cleaning [30]. Muschi et al. [31] experimentally investigated the influence of the oil thickness on the wetting properties and droplet impact dynamics of SLIPS. They observed that the maximum spreading diameter of bouncing droplets on SLIPS followed a $We^{1/4}$ scaling law. Lee et al. [32] explored the effect of the physical properties of the oil and its impact velocity on complex liquid dynamics during the droplet's impact on SLIPS. They concluded that a low-viscosity oil layer was easily displaced by the impacting droplet, resulting in a residual mark in the impact zone and an early onset of prompt splashing. A similar behavior has been reported by the other researchers [33,34], but only a limited literature is available regarding the droplet impact behavior on SLIPS under elevated temperature conditions, emphasizing the need for more in-depth investigations. Numerous fundamental challenges have emerged: There are a lot of impact behaviors of droplets on conventional surfaces as the temperature rises, and whether SLIPS also possess? Can the morphology of SLIPS have a further influence on the above-questioned points?

In this work, a smooth surface, two types of textured surfaces, two types of SLIPS, deionized water, a glycerol–water mixture, and a diesel–water emulsion were selected for the experiments. The static Leidenfrost point (SLFP) of various liquids on different surfaces was quantified, and the impact behavior and the dynamic Leidenfrost point (DLFP) of droplets with substrate temperature $T = 130–230$ °C and impact velocity $V = 0.9–2.8$ m/s were demonstrated. The tilt-impact test demonstrated the advantages of SLIPS for self-cleaning on high-temperature surfaces. Velocity, temperature, and impact behaviors have been presented as impact mode maps. The temperature and velocity fields were simulated by COMSOL Multiphysics 6.2, which predicted the disparities in heat transfer across various surfaces, and the velocity field dynamics elucidated the underlying mechanisms driving the explosive bounce (the rapid rebound driven by localized vapor pressure). Importantly, the thermal resistance and heat transfer of different surfaces were modelled. This study innovatively investigates the impact behavior of droplets on high-temperature SLIPS, addressing the current research gap regarding oil–water mixtures and emulsions. It

further enriches the theoretical understanding of SLIPS in thermal management and holds promise for advancing their applications in spray cooling and droplet condensation.

2. Materials and methods

2.1. Test liquid

Three types of liquids were used during this research work, they were deionized water (CAS 7732-18-5, Type I, resistivity ≥ 18.2 MΩ·cm), the mixture consisted of deionized water and glycerin (mass fraction of glycerol = 2 wt%), and the emulsion consisted of deionized water, diesel fuel (15 W–40), and surfactant (span80), and their mass fractions were 97 wt%, 2 wt%, and 1 wt%, respectively. Both the mixture and the emulsion were stirred for 10 min using a magnetic stirrer. The lubricant used in SLIPS was silicone oil. The physical parameters are shown in Table 1.

2.2. Fabrication of the SLIPS

The substrate ($18 \times 10 \times 3$ mm) was aluminum alloy purchased from Suzhou Metal Material Manufacturer, and the solution used for the chemical modification was a homogeneous mixture of 99 wt% anhydrous ethanol (purity = 95 %) and 1 wt% 1H,1H,2H,2H–Perfluorodecyltrimethoxysilane ($C_{13}H_{13}F_{17}O_3Si$, purity = 99 %). The liquids in Table 1 were purchased from Dow Corning, while anhydrous ethanol and 1H,1H,2H,2H-Perfluorodecyltrimethoxysilane were obtained from Nanjing Middle East Chemical Glass Co. and Aladdin, respectively. Initially, an ultraviolet laser marking machine (KY-M-UV3L, Wuhan Keyi, China) was used to fabricate the micro–nano structures at a speed of 1500 mm/s, power of 6 W, and a pulse frequency of 40 kHz. The purpose was to achieve an enhanced adhesion between the lubricant and the solid surface. The width and depth of the gullies in $Texture_A$ were approximately 17 and 5 μm, respectively, and for $Texture_B$, these were 20 and 35 μm, respectively (morphology has been provided in Supplementary Fig. S1a, b). After this, the specimen underwent chemical modification to reduce the surface energy, as observed by the scanning electron microscope (Supplementary Fig. S1c). Several cluster structures and grid-like microarrays were generated on the surface, which contribute to the superhydrophobic property. The chemical modification lasted for 120 min, followed by drying at 100 °C for 60 min.

The silicone oil was uniformly applied to $Texture_A$ and $Texture_B$ to obtain $SLIPS_A$ and $SLIPS_B$ after draining away excess silicone oil. According to the weighing method and the area difference method, the thickness of the oil film on both SLIPS was calculated to be about 25 μm. The specimen was heated to 130°C/230°C for 5 min and then weighed, and the thickness of the oil film was calculated to be 19 μm/6 μm. SLIPS was fabricated after being tilted at an angle of 90° for 2 h. Fig. 1b provides a schematic demonstration of the fabrication process of SLIPS.

2.3. Experimentation

The experiments were conducted using a specially designed droplet impact observation platform, as shown in Fig. 1a. It consisted of a platform for placing the SLIPS, a ceramic heater, a temperature controller, a rail, a syringe, an LED lamp, and a high-speed camera. The droplet volume was fixed at 12 μL, and it was applied with the help of a syringe. The droplet's impact velocity was calculated by the free-fall equation and varied by adjusting the height of the rail, and the droplet impact behavior was recorded with the help of the high-speed camera (i–SPEED 726R, iX Camera, UK), having a frame rate of 5000 fps. The tested surface of the specimen was heated to the desired temperature using a heating platform with a ceramic heating core (± 5 °C), and the droplet impact experiments were performed when the substrate temperature was stabilized at the desired value.

Table 1
Physical parameters of test liquids.

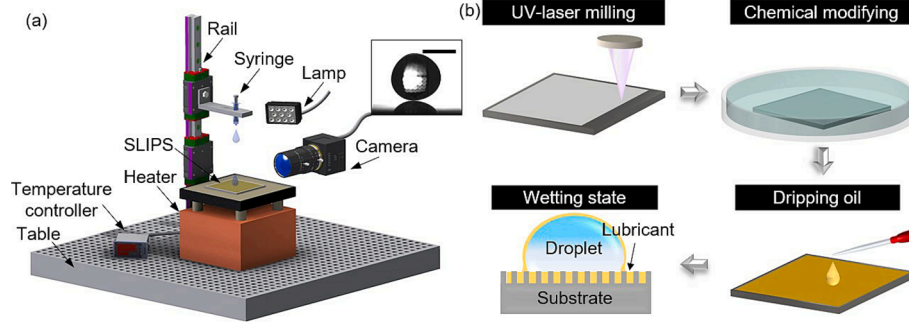|	Deionized water	Glycerin	Diesel fuel	Span 80	Silicone oil	Mixture	Emulsion
Density (kg/m^3)	997	1250	890	1000	963	1005	996
Viscosity (Pa·s)	0.00089	1.49	0.11	1.35	0.01	0.0012	0.0011
Surface tension (N/m)	0.072	0.062	0.03	0.033	0.022	0.0726	0.035
Purity (%)	/	99	99	99	99	/	/
Thermal conductivity (W/(m K))	0.598	0.285	~0.14	~0.17	~0.15	/	/
Specific heat capacity (kJ/(kg·K))	4.18	2.43	~2	~2	~1.5	/	/
Boiling point (°C)	100	290	/	/	~140	/	/

Fig. 1. (**a**) Schematic illustration of the test setup, (**b**) fabrication process for the SLIPS. Scale bars: 1 mm.

The experiments were also conducted to analyze the relationship between temperature and the droplet wettability. The heating device was set to a fixed temperature, and the sample was placed on it for 5 min after thermal equilibrium was reached, and subsequently cooled before measuring the contact angle and sliding angle of droplets. These experiments were performed under ambient environmental conditions, i. e., at 20 °C and atmospheric pressure. Moreover, they were repeated three times to ensure reliability and to calculate the errors.

2.4. Numerical simulation

The temperature and velocity fields were simulated by COMSOL Multiphysics 6.2. Three structures simulating real substrates were designed within a 200 × 70 μm space, as shown in Supplementary Fig. S2. For the temperature field, the top boundary was set as symmetric, while the left and right boundaries were assigned periodically to account for the repetitive pillar arrangement, and the medium in space was water. For the velocity field, the medium was steam, and the top boundary was set as a velocity inlet to simulate the steam generated by evaporation at the bottom of the droplet; the left and right boundaries were defined as pressure outlets. A constant temperature ($T = 130$ °C) was maintained at the bottom boundary in these two physical fields. The liquid heat transfer physical field was employed to simulate the heat transfer at the solid–liquid interface, e.g., conduction, convection, and radiation. The heat transfer equation can be expressed as Eq. (1):

$$\rho_l C_p \frac{\partial T}{\partial t} + \rho_l C_p \mathbf{U} \cdot \nabla T + \nabla \cdot \mathbf{q} = Q \tag{1}$$

$$\mathbf{q} = -k_l \nabla T \tag{2}$$

where $\mathbf{U}$ is the velocity vector, $\mathbf{q}$ is the heat flux vector, Q represents the heat sources other than viscous dissipation, ρ_l is the density of the liquid, C_p is the constant pressure specific heat capacity, and k_l is the thermal conductivity of the liquid. A laminar physical field was applied to calculate the velocity and pressure of single-phase flow under laminar flow conditions, and the interface for calculating laminar flow was based on the general form of the Navier-Stokes equations:

$$\frac{\partial \rho_l}{\partial t} + \nabla \cdot (\rho_l \mathbf{U}) = 0 \tag{3}$$

$$\rho_l \frac{\partial \mathbf{U}}{\partial t} + \rho_l (\mathbf{U} \cdot \nabla) \mathbf{U} = \nabla \cdot [-P\mathbf{I} + \tau] + \mathbf{F} \tag{4}$$

$$\rho_l C_p \left(\frac{\partial T}{\partial t} + (\mathbf{U} \cdot \nabla) T \right) = -(\nabla \cdot \mathbf{q}) + \tau : \mathbf{R} - \frac{T}{\rho_l} \frac{\partial \rho_l}{\partial T}|_P \left(\frac{\partial P}{\partial t} + (\mathbf{U} \cdot \nabla) P \right) + Q \tag{5}$$

$$\mathbf{R} = \frac{\nabla \mathbf{U} + (\nabla \mathbf{U})^T}{2} \tag{6}$$

The continuity equation for the conservation of mass, the vector equation for the conservation of momentum, and the energy conservation equations can be expressed as Eqs. (3), (4), and (5), respectively. Here, P is the pressure, τ is the viscous stress tensor, $\mathbf{F}$ is the volumetric force vector, and $\mathbf{R}$ is the strain rate tensor. The coupling of velocity, pressure, and temperature in the liquid heat transfer field was achieved using a non-isothermal flow multi-physics model.

A transient simulation approach was adopted to predict the evolution of the physical fields over time. For quantifying the thermal timescale, Fourier's law was initially employed to compute the heat flux q and the heat transfer coefficient h_c using Eqs. (7) and (8), respectively [35]:

$$q = \frac{k_s (T_{heater} - T)}{d} \tag{7}$$

$$h_c = \frac{q}{T - T_{sat}} \tag{8}$$

here k_s is the thermal conductivity of the solid, T_{heater} is the temperature of the heating device, $d = 3$ mm is the thickness of the specimen, and T_{sat} is the boiling point of the liquid. Thus, the thermal timescale τ was estimated by Eq. (9) [36]:

$$\tau = \frac{k_l \rho_l C_p}{h_c^2} \tag{9}$$

where k_l and C_p are the thermal conductivity and the specific heat capacity of the liquids, respectively. Based on the experimentally observed temperature difference between the specimen and the heating device, these parameters were estimated as $q = 395$ kW/m^2, $h_c = 13$ kW/(m^2 K),

and $\tau = 14.5$ ms.

For the velocity field, the temperature T at 50 μm height of each simulation domain was selected for the velocity inlet calculation at 14.5 ms. Assuming that the steam enters the computational domain (full of steam initially) vertically from the top and uniformly fills the domain, its initial flow velocity v_n can be expressed by Eq. (10) [37]:

$$v_n = \frac{k_v(T - T_{sat})}{L\rho_v H} \qquad (10)$$

where k_v is the thermal conductivity of the steam, ρ_v is the density of the steam, L denotes the latent heat associated with the phase change, and H corresponds to the height of the simulation domain.

3. Results and discussion

3.1. Wettability characterization, SLFP, thermal stability, and slip experiments

The contact, sliding, advancing, and receding angles of deionized water, glycerol–water mixture, and diesel–water emulsion on the smooth surface, SLIPS$_A$, SLIPS$_B$, and Texture$_A$ have been presented in Fig. 2a, and the specific morphology has been presented in Fig. 2b. It can be seen that the surface structure doesn't influence the wettability performance between SLIPS$_A$ and SLIPS$_B$. The reason for the absence of data for Texture$_B$ is that all the types of liquids spread completely over it, which can be understood as reaching a superhydrophilic state.

Fig. 3a presents the effect of different surfaces on the static Leidenfrost point for water, mixture, and emulsion, by the evaporation time vs. temperature graph at $V = 0$. After an initial decline, a rising trend was observed while exhibiting a distinct inflection point for the smooth surface and SLIPS$_A$. For the smooth surface, liquids can be divided into evaporation, nucleate boiling, transition boiling, and film boiling as described by Liang et al. [38]. However, bubbles adhered to the water–oil interface of SLIPS$_A$ without detachment or bursting. Consequently, only nucleate boiling and film boiling phases could be distinctly identified. The Texture$_A$ exhibited an initial increase followed by a decrease, indicating the presence of both transition boiling and film boiling of droplets. The evaporation time of droplets on SLIPS$_B$ and Texture$_B$ was not sensitive to temperature since they burst quickly, as shown in Fig. 3b. Since the mixture contained only 2 wt% of glycerol, its physical properties closely resemble those of deionized water, and the SLFP of both liquids on the smooth surface, SLIPS$_A$, and Texture$_A$ was 210, 180, and 210 °C, respectively. Due to the influence of oil droplets in the emulsion on water evaporation and the increased difficulty in forming a vapor layer as surface tension decreases, the SLFP of the emulsion for each of the three surfaces was 220, 190, and 220 °C, respectively.

The inclined surface droplet impact experiments were conducted to analyze the performance of SLIPS over other surfaces. The durability of SLIPS$_A$ was evaluated by subjecting the specimen to a controlled thermal environment. Fig. 3c demonstrates that the contact angles of both water and the mixture droplets exhibited a positive correlation with temperature, while fluctuations in the emulsion droplet's contact angle were observed due to its inherent inhomogeneity. Elevated temperatures contributed to the evaporation of the oil film, leading to a negative correlation between temperature and the sliding angles of all three types of droplets. Nevertheless, despite the sliding angle being positively correlated with temperature, they still remained below 4°, confirming the thermal stability of SLIPS$_A$. Fig. 3d compares the slip dynamics of water droplets impacting the smooth surface and SLIPS$_A$ with an inclination angle of 1° and $T = 130$ °C (dynamic processes are provided in Movie S1). A significant sliding was exhibited when the droplet impacted SLIPS$_A$ at $V = 0.9$ m/s, while the droplet on the smooth surface
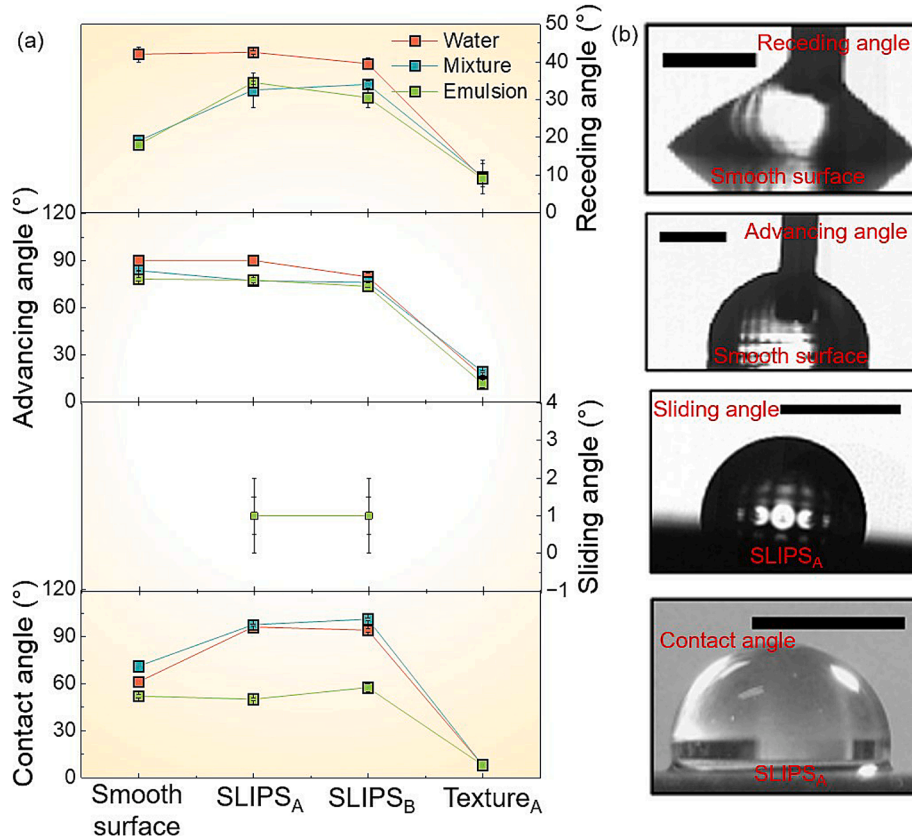

Fig. 2. (a) Wettability characteristics of three liquids on four surfaces with $T = 20$ °C, (b) contact angle, sliding angle, advancing angle, and receding angle of water droplets. Scale bars: 1 mm.
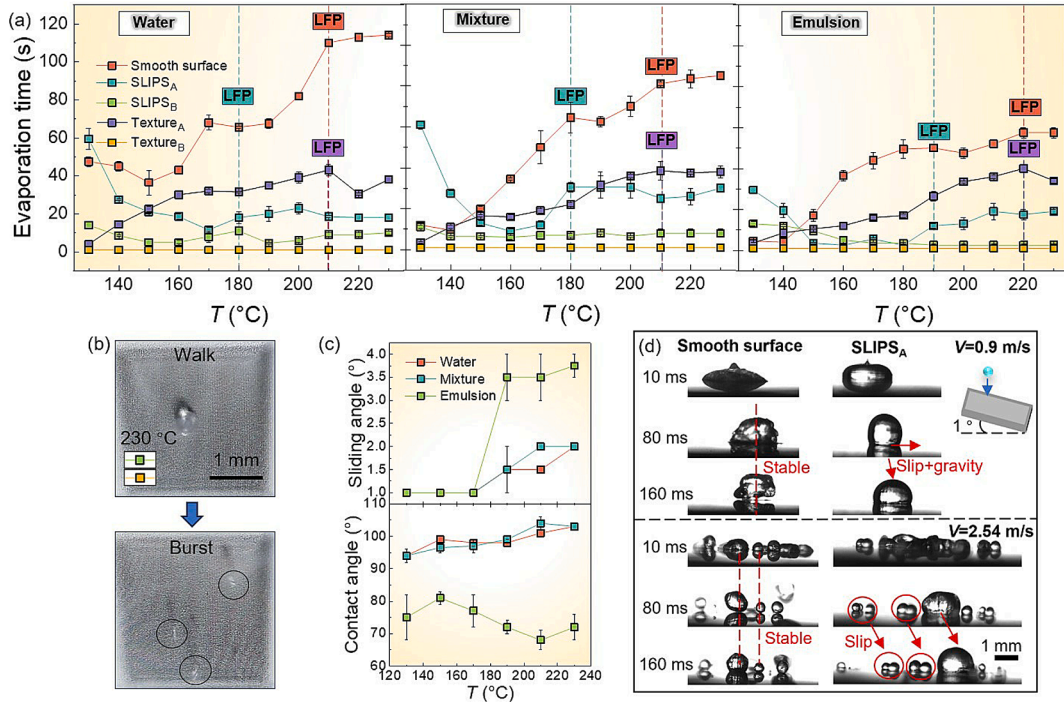
Fig. 3. (**a**) The correlation curve between evaporation time and substrate temperature for water, mixture, and emulsion, (**b**) burst behavior of the droplet on SLIPS$_B$ and Texture$_B$, (**c**) effect of temperature on wettability characteristics of water droplets, (**d**) slip dynamics corresponding to a tilt angle of 1° with $V = 0.9$ m/s and 2.54 m/s.

continued to boil in place. When the impact velocity was increased to 2.54 m/s, the fragmented droplets on SLIPS$_A$ continued to slide downward.

3.2. Impact behaviors and the influence mechanism of the three surfaces

Fig. 4 presents the impact behaviors of water droplets on various surfaces with a velocity, $V = 0.9$ m/s, and the transition from deposit, partial bounce, and explosive bounce to total bounce allows the determination of the DLFP of a droplet at a given velocity. For the smooth and Texture$_A$ surfaces, the droplet demonstrated a transition from deposit to the total bounce at 160 °C, whereas the DLFP on Texture$_B$ was increased up to 190 °C. A similar phenomenon of pancake bouncing was observed on superhydrophobic surfaces patterned with a square lattice of tapered posts [39,40]. Texture$_B$ was a superhydrophilic surface, and a comparison with Texture$_A$ highlighted the crucial role of surface microstructures in governing droplet bounce dynamics. For SLIPS$_A$ and SLIPS$_B$, the total bounce was observed at 130 °C. Although such a low temperature does not typically correspond to the DLFP, it demonstrated that

regardless of the Leidenfrost effect, SLIPS inherently facilitate efficient total bounce of droplets.

Fig. 5 presents the impact mode maps for $V = 0.9$–2.8 m/s and $T = 130$–230 °C, which provide a comprehensive understanding of the impact dynamics across a broader range of impact velocity and temperature intervals. Five impact behaviors were observed, i.e., deposit, partial bounce, total bounce, crush, and explosive bounce (dynamic processes have been demonstrated in supplementary Movie S2). The three types of droplets exhibited a comparable impact behavior on the smooth surface and Texture$_B$, while water and the mixture demonstrated similar dynamics on SLIPS$_A$ and SLIPS$_B$, i.e., all droplets bounced off under $V = 1.53$ m/s. The lower the velocity, the higher the probability that the droplet undergoes total bounce. The DLFP of water droplets on the smooth surface, Texture$_A$, and Texture$_B$ at $V = 0.9$ m/s were similar to the mixture, i.e., 160, 160, and 190 °C, respectively. The emulsion exhibited the impact dynamics on all five surfaces, and the DLFP were 150, 150, 180, 180, and 200 °C, as presented in Fig. 5c. Additionally, the mixture on Texture$_A$ and the emulsion on SLIPS$_B$ demonstrated a lower probability of achieving the total bounce. Hence, water and mixture
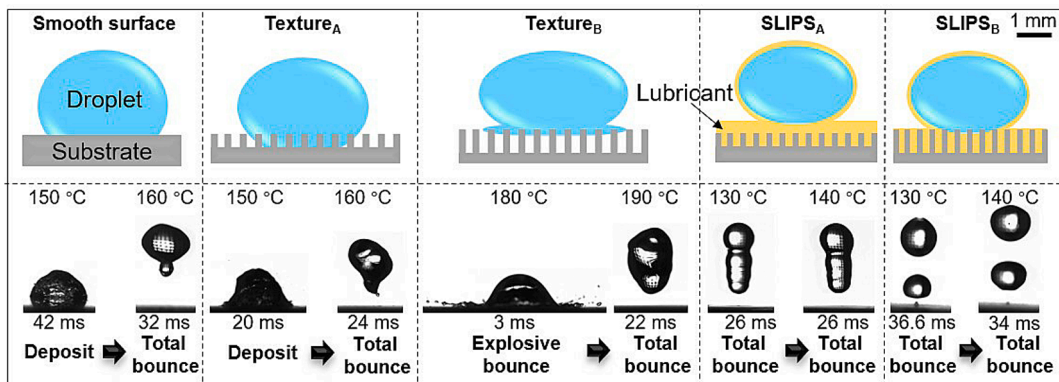

Fig. 4. Impact behavior of water droplets on various surfaces below and above the DLFP ($V = 0.9$ m/s).
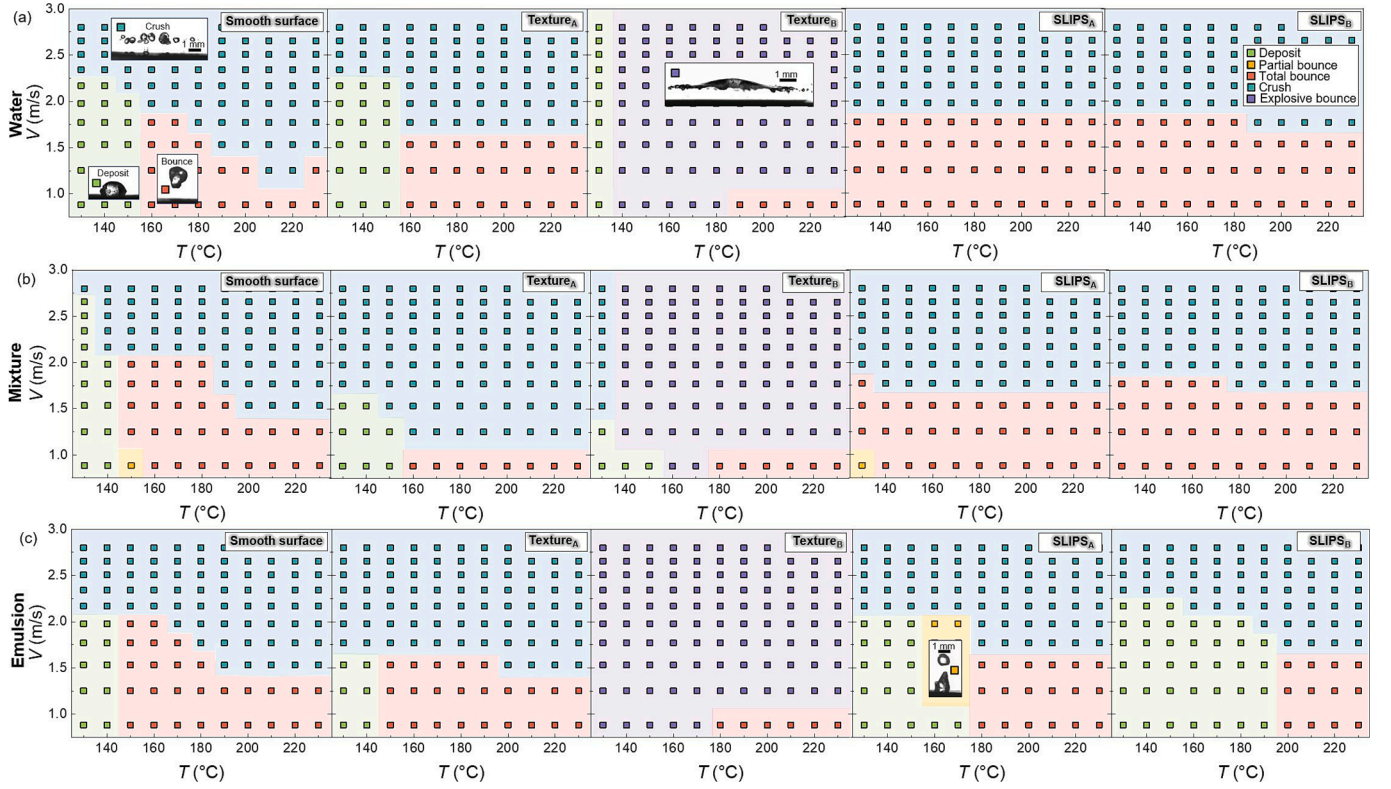
Fig. 5. Impact mode maps for $V = 0.9$–2.8 m/s, $T = 130$–230 °C. (**a**) Water, (**b**) the mixture, (**c**) the emulsion.

droplets demonstrated a lower DLFP on SLIPS than on other surfaces, while emulsion droplets required lower temperatures to achieve the total bounce condition on smooth surfaces than SLIPS. However, the reason why the emulsion shows a higher SLFP [41] is that the addition of diesel fuel leads to the formation of a micro oil film or a water-in-oil

structure at the bottom of the droplet, which hinders local boiling and delays the generation of the vapor film. Although span80 reduces the surface tension, the overall viscosity of the emulsion remains higher than that of deionized water, resulting in suppressed internal convection within the droplet, slower heat transfer, and a reduced likelihood of
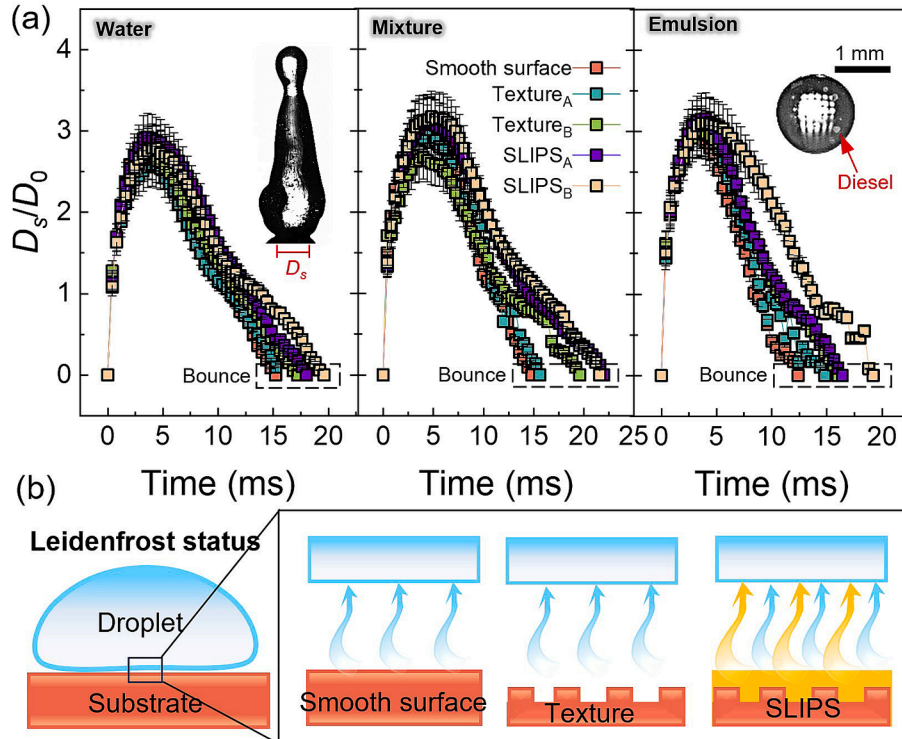

Fig. 6. (**a**) Variation of D_s/D_0 with time under $T = 230$ °C and $V = 0.9$ m/s, (**b**) schematic of vapor flow on different surfaces.

achieving local superheating at the droplet base.

A comparison of the spreading behavior of droplets on different surfaces explained the phenomenon of reduction in the DLFP of droplets by SLIPS. Fig. 6a presents the temporal evolution of the ratio of the droplet's spreading diameter D_s to its initial diameter D_0 on various surfaces under Leidenfrost status ($T = 230\ ^\circ\text{C}$). Water, the mixture, and the emulsion droplets exhibited the highest D_s/D_0 and correspondingly the longest bouncing duration on SLIPS$_A$ and SLIPS$_B$, followed sequentially by Texture$_B$, Texture$_A$, and the smooth surface. This indicated that the gas film on SLIPS$_A$ and SLIPS$_B$ provided stronger support to the droplet. On smooth surfaces, even when the Leidenfrost effect occurs, the droplet base is not entirely separated from the surface (from the light interference image [42]), leading to persistent contact line pinning during spreading. In contrast, this issue is absent on the SLIPS, where the combined evaporation of lubricant and water enables more complete droplet spreading and increases the likelihood of rebound. Due to the slightly increased viscosity, the bounce of the mixture required a longer time, as more kinetic energy was converted into viscous dissipation. Additionally, the inhomogeneity of oil molecules in the emulsion caused more pronounced fluctuations during the retraction phase. Fig. 6b demonstrates that when a droplet bounces off SLIPS, it is propelled by both its evaporation and the evaporation of the oil film when compared with the smooth and textured surfaces. Moreover, owing to the significantly reduced liquid sliding resistance on SLIPS, droplets underwent enhanced spreading while still retaining their ability to bounce. The difference in how surface structure influences droplet impact behavior is clearly evident between Texture$_A$ and Texture$_B$. As shown in Fig. 5, explosive bounce occurs exclusively on Texture$_B$. From Fig. 6b, it can be observed that the deeper microstructures of Texture$_B$ severely obstruct the flow of vapor generated by evaporation beneath the droplet, creating multiple localized vortices. These vortices increase local pressure, which rapidly forces the droplet base to expand outward in all directions, resulting in an explosive bounce. In contrast, Texture$_A$ possesses shallower microstructures that exert less influence on vapor flow, allowing the droplet to spread more stably upon impact.

3.3. Numerical simulation

Numerical simulations were conducted to understand the effect of different surfaces, i.e., smooth surface, Texture$_A$, Texture$_B$, on the heat transfer and steam flow between solid and liquid, and to analyze the variations in temperature and velocity field distributions. Fig. 7a illustrates the temperature T_d at different distances from the bottom at 14.5 ms, where the bottom boundary was fixed at 130 °C, and the relevant boundary settings for the simulation have been provided as Supplementary Fig. S2. The inset figures demonstrate that water in the simulation domain warms up faster in Texture$_B$ due to its larger solid–liquid contact area. The bottom of the droplet experienced rapid heating upon impacting Texture$_B$, and the presence of gaps within the arrayed microstructure facilitated the short-term accumulation of localized high pressure, thereby promoting the onset of explosive bounce.

The flow behavior was significantly influenced by the surface structure when evaporation from the water droplet's bottom generated the steam flow. According to Eq. (10), the entrance velocities of the three structural simulation domains were $v_n = 0.049$, 0.053, and 0.08 m/s, respectively. Fig. 7b presents the velocity and pressure field distribution for the smooth, Texture$_A$, and Texture$_B$ surfaces. From the velocity field at 14.5 ms, the streamlined distribution over both the smooth and Texture$_A$ surfaces exhibited a relatively symmetric pattern, with steam diffusing radially outward from the top. Although Texture$_A$ contained surface protrusions, their geometric features were insufficient to significantly disturb the underlying flow, resulting in minimal deviation of the bottom streamlines. In contrast, Texture$_B$ featured deeper and more pronounced structural elements, which induced the formation of localized eddy currents and the localized acceleration at the top of the pillars. Hence, a non-uniform steam pressure was built within the confined spaces, and the highest pressure was developed at the middle of the pillars on Texture$_B$, which contributed to the onset of explosive bounce in the impacting droplet (independently scaled velocity and pressure ranges have been provided as Supplementary Fig. S3).

Fig. 8a presents the time-resolved evolution of impact behaviors of different liquid droplets on Texture$_B$. At $T = 140°\text{C}$ and $V = 0.9$ m/s, both the emulsion and water droplets exhibited an explosive bounce. However, the inherent inhomogeneity of the emulsion [43] resulted in an asymmetric morphology compared to the water droplet at 1.4 ms. Due to a higher viscosity than water, the mixture remained deposited at the surface rather than bouncing. At $V = 2.8$ m/s, the droplet exhibited explosive bounce at 0.6 ms, and the final symmetric spread position was lower than that observed at 0.9 m/s, suggesting that higher impact velocity leads to a greater vapor pressure buildup beneath the droplet. At T
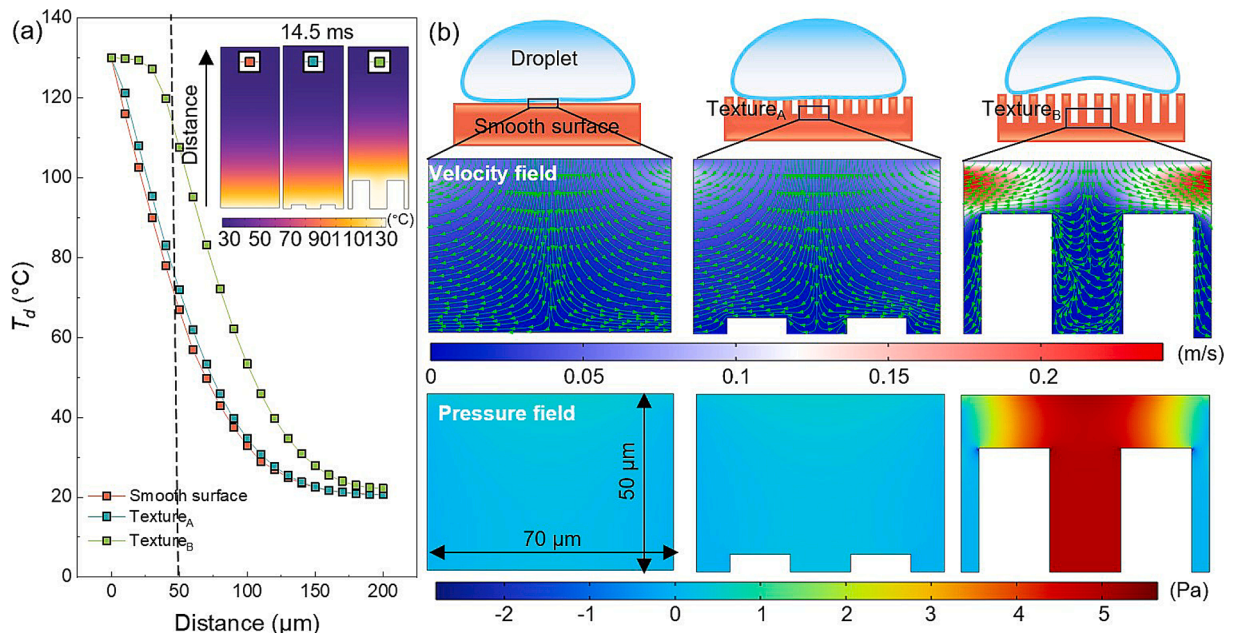

Fig. 7. (**a**) Vertical temperature distribution at 14.5 ms, (**b**) velocity and pressure field at 14.5 ms.
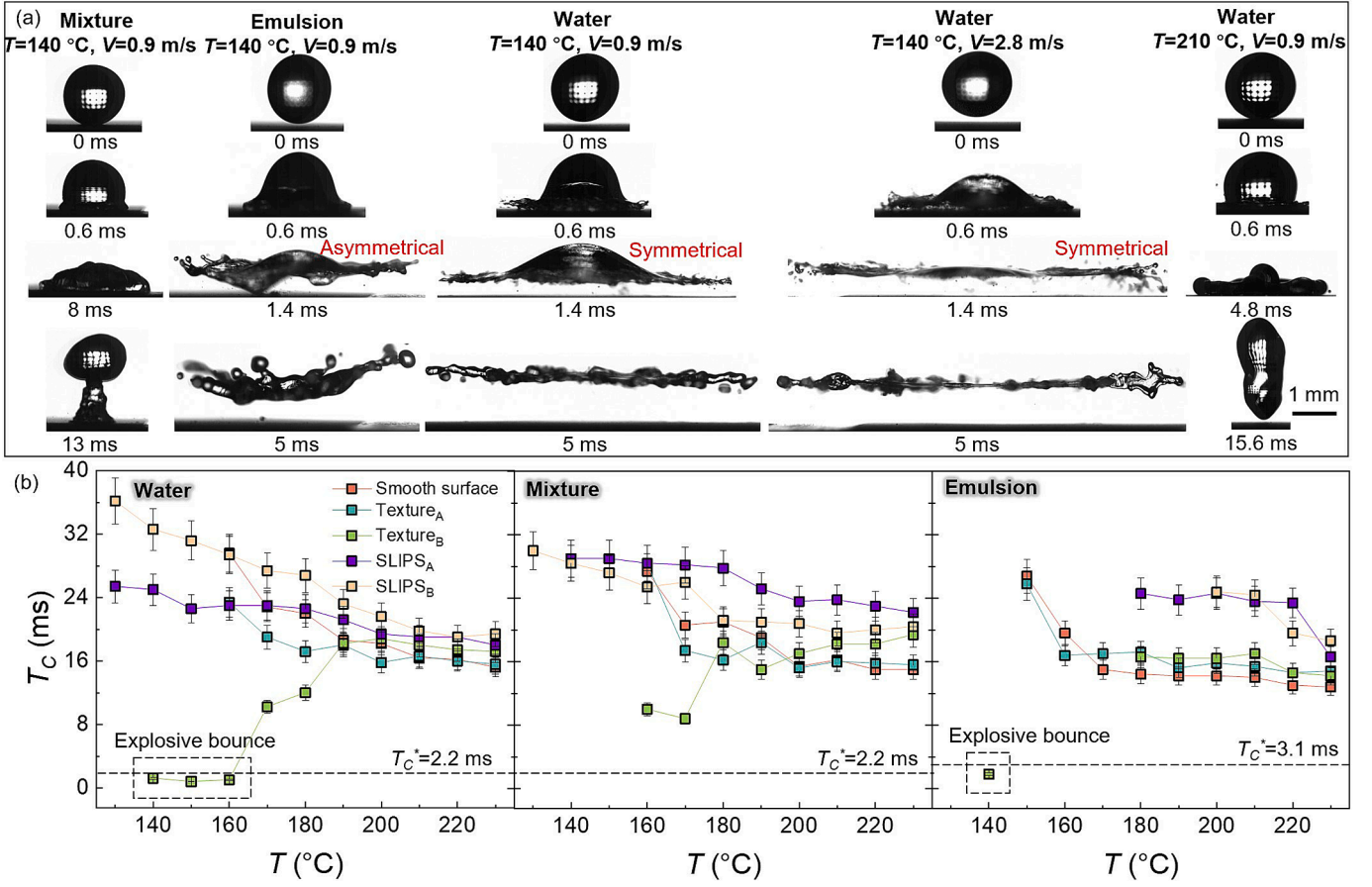
Fig. 8. (a) Changes in droplet behavior over time on Texture_B, (b) solid–liquid contact time corresponding to $V = 0.9$ m/s.

= 210 °C and $V = 0.9$ m/s, the droplet bounced off the surface at 15.6 ms, whereas the explosive bounce occurred within 1.4 ms or even less, indicating a significant reduction in the characteristic timescale of the process. Fig. 8b presents the relationship between solid–liquid contact time T_c and T, and the theoretical Rayleigh limit T_c^* was considered to illustrate the shortest contact time that can be achieved after a droplet

impacts the surface [17]. It can be expressed as Eq. (11):

$$T_c^* = \sqrt{\frac{\rho_l R^3}{\gamma_l}} \tag{11}$$

where ρ_l and γ_l represent the density and surface tension of the liquid,
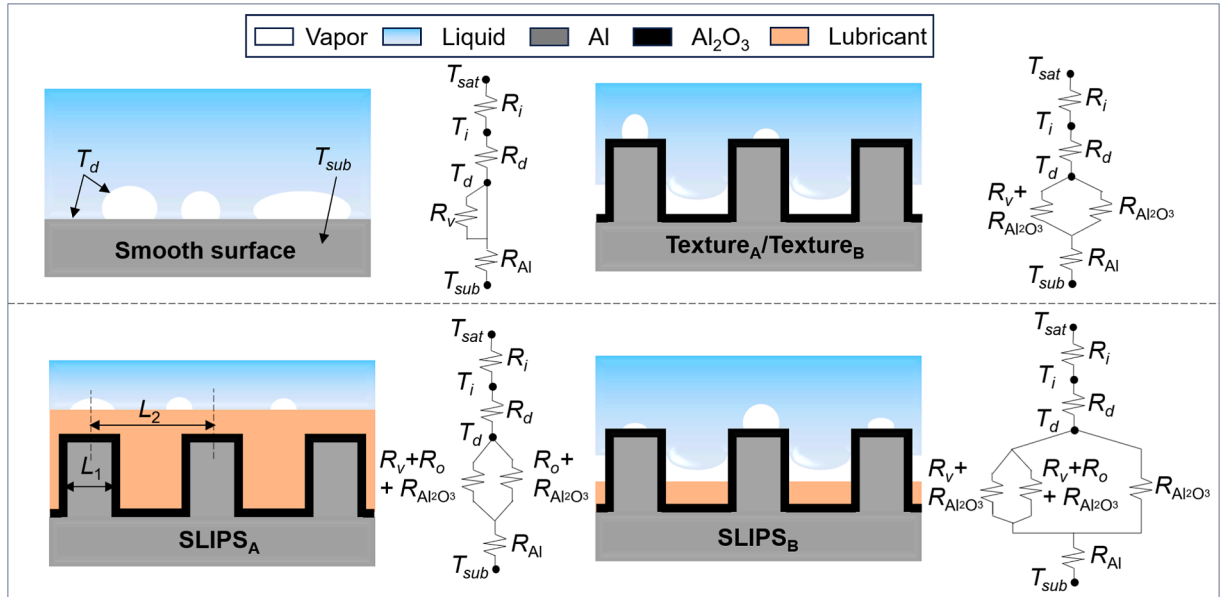

Fig. 9. Thermal resistance modelling of five surfaces.

respectively, and R denotes the initial radius of the droplet. The corresponding T_c* for water, the mixture, and the emulsion were found to be 2.2, 2.2, and 3.1 ms, respectively. From Fig. 8b, it was observed that T_c of the droplets was negatively correlated with T on all surfaces except Texture$_B$, while T_c corresponding to the explosive bounce occurring on Texture$_B$ was lower than T_c* in all cases. The theoretical Rayleigh limit represents the fastest bounce time of a droplet dominated by its own inertia and surface tension during the impact process without additional external forces (e.g., surface structure, external airflow, etc.). The comparison between Texture$_B$ and SLIPS$_B$ revealed that the microstructure of Texture$_B$ exceeded the classical Rayleigh oscillation time limit, significantly reducing T_c.

3.4. Model of the interfacial thermal resistance and heat transfer coefficients for all surfaces

Based on the size parameters of micro-nano textures introduced in Section 2.2 and the oil film thickness during operation, Fig. 9 depicts the heat transfer and thermal resistance models of five surfaces [44,45]. Here, T_{sat}, T_i, T_d, and T_{sub} denote the saturation temperature of water, the temperature of the top edge of the droplet, the bottom edge of the droplet, and the substrate, respectively; R_i, R_d, R_v, and R_o represent the interfacial thermal resistances of condensation, droplet, vapor, and lubricant, respectively; R_{Al} and $R_{Al_2O_3}$ correspond to the interfacial thermal resistances of Al and Al$_2$O$_3$, respectively. Therefore, the heat transfer through a single droplet can be formulated as:

$$q_{smooth} = \frac{T_{sat} - T_{sub}}{R_i + R_d + R_v + R_{Al}} \tag{12}$$

$$q_{Texture} = \frac{T_{sat} - T_{sub}}{R_i + R_d + R_v + R_{Al} + R_{Al_2O_3}} \tag{13}$$

$$q_{SLIPS_A} = \frac{T_{sat} - T_{sub}}{R_i + R_d + R_v + R_o + R_{Al} + R_{Al_2O_3}} \tag{14}$$

$$q_{SLIPS_B} = \frac{T_{sat} - T_{sub}}{R_i + R_d + R_v + \varphi R_o + (1-\varphi)R_{Al_2O_3} + R_{Al}} \tag{15}$$

where q_{smooth}, $q_{Texture}$, q_{SLIPSA}, and q_{SLIPSB} denote the heat transfer of the smooth surface, Texture$_A$/Texture$_B$, SLIPS$_A$, and SLIPS$_B$, respectively, and φ is the percentage of area covered by lubricant. The interfacial thermal resistance is calculated as:

$$R_i = \frac{1}{2\pi r^2 h_i (1-\cos\theta_a)}, h_i = \frac{2\alpha\rho_v L^2}{(2-\alpha)T_{sat}\sqrt{2\pi R_g T_{sat}}} \tag{16}$$

here, r and θ_a represent the radius and advancing angle of the droplet, respectively; h_i is an important heat transfer coefficient, and α and R_g are the accommodation coefficient function and the specific gas constant, respectively. What's more, let δ_o and k_o be the thickness and thermal conductivity of the lubricant, R_d and R_o can be expressed as:

$$R_d = \frac{\theta_a}{4\pi r k_l \sin\theta_a}, R_o = \frac{\delta_o}{\pi r^2 k_o \sin^2\theta_a} \tag{17}$$

In contrast, the thermal resistance on both SLIPS$_A$ and SLIPS$_B$ is slightly increased, mainly in the lubricant, and is directly influenced by the microstructure size. For the effective heat transfer coefficient k_{eff}, we first revisit the heat transfer model shown in Fig. 9. For the smooth surface, k_{eff} is denoted as k_s. Considering that L_1 and L_2 represent the dimensional parameters of the microstructures, surfaces featuring microstructures, such as Texture$_A$ and Texture$_B$, can be analyzed using the approach described in [17]:

$$k_{eff} = k_s \left(\frac{L_1}{L_2}\right)^2 + k_v \left[1 - \left(\frac{L_1}{L_2}\right)^2\right] \tag{18}$$

where k_s and k_v are the thermal conductivities of substrate and vapor, respectively. Since SLIPS$_A$ is completely covered by the lubricant, $k_{eff} = k_o$. For SLIPS$_B$, it is similar to the textured surfaces, which can also be expressed by Eq. (18). Therefore, the thermal conductivity coefficients of various surfaces are presented in Table S1.

4. Conclusion

This research work presents an experimental investigation to analyze the effect of high-temperature environments on the droplet impact behavior on slippery liquid-infused porous surfaces (SLIPS). Water, water–glycerol mixture, and water–diesel emulsion were selected as the working liquids. The smooth and textured surfaces were included for comparative analysis with SLIPS under identical thermal and dynamic conditions.

Droplet evaporation experiments demonstrated that SLIPS$_A$ significantly reduces SLFP for water, mixture, and emulsion observed at 180, 180, and 190 °C, respectively, which is 30 °C lower than both the smooth surface and Texture$_A$. The advantage of SLIPS in reducing SLFP enhances their application in the field of high-temperature droplet manipulation. What's more, the thermal stability of SLIPS was convincingly demonstrated, while slip experiments further underscored their potential for high-temperature self-cleaning applications. The explosive bounce behavior of droplets on Texture$_B$ was found to significantly reduce the solid–liquid contact time, which exhibited a clear negative correlation with temperature across all tested liquids, indicating that elevated surface temperatures enhance the rapid vapor generation.

Numerical simulations revealed distinct differences in thermal transport characteristics across various surface structures. These simulations elucidated the underlying mechanisms driving explosive bounce, highlighting the role of structural geometry in modulating heat transfer and vapor flow at the droplet–substrate interface. Overall, the interfacial contact mechanisms (related features such as DLFP, impact behaviors) between water, mixture, emulsion and smooth surface, textured surfaces, and SLIPS were well described, while innovative approaches were employed to model thermal resistance and heat transfer behavior on different surfaces. However, practical challenges remain for real-world applications of SLIPS, particularly the durability of the infused lubricant under repeated high-temperature cycles, where lubricant depletion and thermal degradation could limit long-term performance. Future work should investigate the lifetime and robustness of SLIPS under cyclic thermal loads, as well as strategies for lubricant replenishment or thermally stable lubricant formulations. Additionally, SLIPS show great promise for industrial applications such as spray cooling systems and condensation, where achieving a low Leidenfrost point is critical to enhance heat transfer efficiency and operational safety under extreme thermal conditions.

CRediT authorship contribution statement

Chuchen Yue: Writing – review & editing, Writing – original draft, Software, Methodology, Investigation. **Qingwen Dai:** Writing – review & editing, Funding acquisition, Conceptualization. **Wei Huang:** Supervision, Project administration, Methodology. **Xiaolei Wang:** Supervision, Project administration, Methodology.

Declaration of competing interest

The authors declare that they have no known competing financial interests or personal relationships that could have appeared to influence the work reported in this paper.

Appendix A. Supplementary material

Supplementary data to this article can be found online at https://doi.org/10.1016/j.applthermaleng.2025.127650.

Data availability

Data will be made available on request.

References

[1] Y. Wang, N. Hu, Y. Zhang, R. Song, L. Liu, X. Zhao, G. Cheng, N. Yuan, J. Ding, A slippery liquid-infused porous surface with self-cleaning and liquid-repellent properties, long-term corrosion resistance, and high mechanical stability, Colloid Surf. A 723 (2025) 137362.

[2] H. Fukuda, Y. Kita, T. Ariyoshi, Y. Takata, M. Kohno, Experimental investigation of spray cooling on steel plates with periodic micropillar structures: two-stage quenching phenomenon, Appl. Therm. Eng. 275 (2025) 126870.

[3] X. Gao, R. Li, Impact of a drop burst flow on a film flow cooling a hot surface, Int. J. Heat Mass Transf. 126 (2018) 1193–1205.

[4] Q. Dai, W. Huang, X. Wang, M.M. Khonsari, Directional interfacial motion of liquids: fundamentals, evaluations, and manipulation strategies, Tribol. Int. 154 (2021) 106749.

[5] Q. Dai, C. Du, W. Huang, X. Wang, Regulation of liquid self-transport through architectural-thermal coupling: transitioning from free surfaces to open channels, Adv. Sci. 12 (2025) 2412483.

[6] C. Yue, Q. Dai, W. Huang, X. Wang, Droplets bouncing on rotating curved surfaces with elevated temperatures, Int. J. Heat Mass Transf. 215 (2023) 124479.

[7] Y. Guo, X. Liu, J. Ji, Z. Wang, X. Hu, Y. Zhu, J. Wang, Y. Du, K. Liu, Y. Jiao, Suppressed Leidenfrost effect on the rough tool surface with negative skewness for high-efficiency evaporation cooling, Appl. Therm. Eng. 242 (2024) 122445.

[8] D. Quéré, Leidenfrost dynamics, Annu. Rev. Fluid Mech. 45 (2013) 197–215.

[9] Q. Ma, X. Wu, T. Li, F. Chu, Droplet boiling on heated surfaces with various wettabilities, Appl. Therm. Eng. 167 (2020) 114703.

[10] C. Cai, I. Mudawar, Review of the dynamic Leidenfrost point temperature for droplet impact on a heated solid surface, Int. J. Heat Mass Transf. 217 (2023) 124639.

[11] T. Tran, H.J.J. Staat, A. Prosperetti, C. Sun, D. Lohse, Drop impact on superheated surfaces, Phys. Rev. Lett. 108 (2012) 036101.

[12] C. Guo, D. Maynes, J. Crockett, D. Zhao, Heat transfer to bouncing droplets on superhydrophobic surfaces, Int. J. Heat Mass Transf. 137 (2019) 857–867.

[13] D.-Q. Wang, Z.-J. Wang, S.-Y. Wang, Y.-F. Wang, Y.-R. Yang, S.-F. Zheng, B. Gao, X.-D. Wang, A molecular dynamics study of droplet impact dynamics on the heated pyramid-shaped surface, Int. J. Heat Mass Transf. 251 (2025) 127339.

[14] J. Zhang, W. Zhao, H. Liu, D. Wang, H. Cui, L. Chen, Numerical study of droplets impacting on flat and cone-arrayed surfaces, Int. Commun. Heat Mass 163 (2025) 108729.

[15] S. Mitra, M.J. Sathe, E. Doroodchi, R. Utikar, M.K. Shah, V. Pareek, J.B. Joshi, G. M. Evans, Droplet impact dynamics on a spherical particle, Chem. Eng. Sci. 100 (2013) 105–119.

[16] W. Zhang, T. Yu, J. Fan, W. Sun, Z. Cao, Droplet impact behavior on heated micro-patterned surfaces, J. Appl. Phys. 119 (2016) 114901.

[17] M. Liu, H. Du, Y. Cheng, H. Zheng, Y. Jin, S. To, S. Wang, Z. Wang, Explosive pancake bouncing on hot superhydrophilic surfaces, ACS Appl. Mater. Interfaces 13 (2021) 24321–24328.

[18] Y. Guo, X. Liu, J. Ji, J. Wang, Y. Du, K. Liu, Y. Jiao, Achieving wide temperature range of gentle film boiling on textured hydrophobic tool surfaces, Phys. Fluids 36 (2024) 112113.

[19] Y. Guo, X. Liu, J. Ji, Z. Wang, X. Hu, Y. Zhu, T. Zhang, T. Tao, K. Liu, Y. Jiao, Delayed Leidenfrost effect of a cutting droplet on a microgrooved tool surface, Langmuir 39 (2023) 9648–9659.

[20] Y. Jiao, J. Wang, Y. Guo, Y. Du, Y. Zhu, J. Ji, X. Liu, K. Liu, Effect of the surface peak–valley features on droplet impact dynamics under Leidenfrost temperature, Langmuir 40 (2024) 20773–20782.

[21] N. Blanken, M.S. Saleem, C. Antonini, M.-J. Thoraval, Rebound of self-lubricating compound drops, Sci. Adv. 6 (2020) eaay3499.

[22] C. Cai, H. Chen, H. Liu, C. Si, Effect of iso-propanol additive on the impact dynamics of a Leidenfrost water droplet, Appl. Therm. Eng. 234 (2023) 121326.

[23] M. Damak, J. de Ruiter, S. Panat, K.K. Varanasi, Dynamics of an impacting emulsion droplet, Sci. Adv. 8 (2022) eabl7160.

[24] E. Mura, P. Massoli, C. Josset, K. Loubar, J. Bellettre, Study of the micro-explosion temperature of water in oil emulsion droplets during the Leidenfrost effect, Exp. Therm Fluid Sci. 43 (2012) 63–70.

[25] T. Wong, S.H. Kang, S.K.Y. Tang, E.J. Smythe, B.D. Hatton, A. Grinthal, J. Aizenberg, Bioinspired self-repairing slippery surfaces with pressure-stable omniphobicity, Nature 477 (2011) 443–447.

[26] S. Sett, P. Sokalski, K. Boyina, L. Li, K.F. Rabbi, H. Auby, T. Foulkes, A. Mahvi, G. Barac, L.W. Bolton, N. Miljkovic, Stable dropwise condensation of ethanol and hexane on rationally designed ultrascalable nanostructured lubricant-infused surfaces, Nano Lett. 19 (2019) 5287–5296.

[27] R. Gulfam, Z. Deng, Y. Ishrat, I.I. Cheema, Y. Lu, T.-E. Huang, F. Lv, S. Wu, Condensation dynamics, heat transfer and energy-exergy analyses on slippery-liquid infused copper nanowires, Appl. Therm. Eng. 269 (2025) 126058.

[28] B. Qi, X. Yang, X. Wang, Ultraslippery/hydrophilic patterned surfaces for efficient fog harvest, Colloid Surf. A 640 (2022) 128398.

[29] K. Zhuang, Y. Lu, X. Wang, X. Yang, Architecture-driven fast droplet transport without mass loss, Langmuir 37 (2021) 12519–12528.

[30] C. Yue, Q. Dai, X. Yang, C. Gachot, W. Huang, X. Wang, Controllable self-transport of bouncing droplets on ultraslippery surfaces with wedge-shaped grooves, Droplet 3 (2024) e118.

[31] M. Muschi, B. Brudieu, J. Teisseire, A. Sauret, Drop impact dynamics on slippery liquid-infused porous surfaces: influence of oil thickness, Soft Matter 14 (2018) 1100–1107.

[32] C. Lee, H. Kim, Y. Nam, Drop impact dynamics on oil-infused nanostructured surfaces, Langmuir 30 (2014) 8400–8407.

[33] S. Hanosh, S.D. George, Substrate viscosity-dependent droplet behavior on slippery surface, Colloid Surf. A 706 (2025) 135811.

[34] J. Kim, J.P. Rothstein, Droplet impact dynamics on lubricant-infused superhydrophobic surfaces: the role of viscosity ratio, Langmuir 32 (2016) 10166–10176.

[35] D.I. Shim, W. Hsu, M. Yun, D. Lee, B.S. Kim, H.H. Cho, Superbiphilic patterned nanowires with wicking for enhanced pool boiling heat transfer, Int. J. Mech. Sci. 249 (2023) 108280.

[36] W. Huang, L. Zhao, X. He, Y. Li, C.P. Collier, Z. Zheng, J. Liu, D.P. Briggs, J. Cheng, Low-temperature Leidenfrost-like jumping of sessile droplets on microstructured surfaces, Nat. Phys. 20 (2024) 1274–1281.

[37] G.G. Wells, R. Ledesma-Aguilar, G. McHale, K. Sefiane, A sublimation heat engine, Nat. Commun. 6 (2015) 6390.

[38] G. Liang, I. Mudawar, Pool boiling critical heat flux (CHF) – Part 1: Review of mechanisms, models, and correlations, Int. J. Heat Mass Transf. 117 (2018) 1352–1367.

[39] Y. Liu, L. Moevius, X. Xu, T. Qian, J.M. Yeomans, Z. Wang, Pancake bouncing on superhydrophobic surfaces, Nat. Phys. 10 (2014) 515–519.

[40] H. Wu, K. Jiang, Z. Xu, S. Yu, X. Peng, Z. Zhang, H. Bai, A. Liu, G. Chai, Theoretical and experimental studies on the controllable pancake bouncing behavior of droplets, Langmuir 35 (2019) 17000–17008.

[41] G.V.V.S.V. Prasad, P. Dhar, D. Samanta, Postponement of dynamic Leidenfrost phenomenon during droplet impact of surfactant solutions, Int. J. Heat Mass Transf. 189 (2022) 122675.

[42] Y. Liu, Y. Zheng, Y. Zhou, W. Zhao, Y. Li, S. Tang, C. Wang, S. Wang, Y. Chai, P. Zhu, Self-lubricated bouncing of hot droplets, Newton 1 (2025) 100014.

[43] M.Y. Khan, Z.A. Abdul Karim, A.R.A. Aziz, I.M. Tan, Experimental investigation of microexplosion occurrence in water in diesel emulsion droplets during the leidenfrost effect, Energy Fuel 28 (2014) 7079–7084.

[44] Y. Maeda, F. Lv, P. Zhang, Y. Takata, D. Orejon, Condensate droplet size distribution and heat transfer on hierarchical slippery lubricant infused porous surfaces, Appl. Therm. Eng. 176 (2020) 115386.

[45] Y.S. Yogi, H.B. Parmar, H. Fattahi Juybari, S. Nejati, A.K. Rao, R. Roy, M. Zarei, L. Li, S. Sett, A. Das, N. Miljkovic, J.A. Weibel, D.M. Warsinger, Slippery liquid infused porous surface (SLIPS) condensers for high efficiency air gap membrane distillation, Commun. Eng. 4 (2025) 48.